# Hydrogen production using mixed oxides: TiO2-M (CoO and $WO_3$)

Alejandro Pérez-Larios[1,2]*; Ricardo Gómez[1].

[1]*Universidad Autónoma Metropolitana-Iztapalapa, Depto. de Química, Área de Catálisis, Grupo ECOCATAL, Av. San Rafael Atlixco No 189, México 09340, D.F. México. *alex.perez.larios@gmail.com*

[2]*Universidad de Guadalajara, Centro Universitario de Tonalá, División de Ingenierias, Sede Provisional Casa de la Cultura – Administración: Morelos # 180, Zona Centro, Tonalá, Jalisco, México. 45400*

*Fecha de recepción del artículo: 24/06/2013 Fecha de aceptación del artículo: 10/07/2013*

## Abstract

In this work we obtained materials of titanium dioxide whit mixed oxide CoO-TiO2 and WO3-TiO2 (1.0, 3.0, 5.0 %wt). The solids were characterized by; nitrogen physisorption (BET) and porosity (BJH), XRD patterns and UV-Vis spectroscopy. The photoactivity was evaluated using a Pyrex reactor of 200 ml using a solution ethanol-water (1:1 molar ratio) and 0.1 g of catalyst using a high pressure Hg lamp (with a wavelength of 254 nm and an intensity of 2.2 mW/cm$^2$ encapsulated in a quartz tube. The results showed materials with specific surface area among 89 to 95 m2/g and 41 to 91 m$^2$/g with mesopority characteristics. The XRD patterns show the formation of the crystalline anatase phase. The band gap energy (Eg) for the materials were obtained with UV-Vis spectroscopy, the Eg values were lower than 3.2 eV for both mixed oxide. In the water splitting evaluation a maxim in the efficient was found at Co and W at 5 wt.%. The hydrogen produced was 1000 µmol/h and 950 µmol/h respectively, this is a value comparable to respect other works.

## Keywords

Hydrogen production, Mixed oxide, Sol gel, Photocatalysts, UV-vis.

## 1. Introduction

An important process for future energy supplies turns to be "photohydrogen" production from water splitting; the photocatalytic processes is clean and employ a renewable source as it has been reported for various systems [1-3]. Titanium dioxide ($TiO_2$) is considered as the best photocatalysts for dyes degradation [4-9] pesticides [10-14] atmospheric pollutants [15] as well as for the inorganic pollutant removal from wastewater [16,17]. However, the use of $TiO_2$ as photocatalysts for water splitting is limited by its redox potential referring to the normal hydrogen electrode (NHE). Important studies have been made to improve the photocatalytic activity of titanium dioxide for the water splitting reaction. In this way, modified titanium dioxide prepared by doping with Fe, Zn, Cu, Ni, V, Mg, Be and Ni [18,19], or by impregnating the $TiO_2$ with noble metals Pt, Pd, Ir, Rh, Ru [20]. In particular, the preparation of mixed oxides like CuO, ZnO, NiO and CeO [21-24], has attracted attention for researchers because they are low cost materials showing important photocatalytic properties. The incorporated oxide effect has been related to oxygen vacancies in its crystal structure [25,26]. With the propose to obtain improved titania photocatalysts with high hydrogen production from water splitting, in the

present work $TiO_2$-CoO and $TiO_2$-$WO_3$ mixed oxides were prepared by the sol-gel method. Cobalt oxide and tungsten trioxide has been chosen as co-participant oxide because its energetic conduction and valence bands positions are in the favorable redox region for the water splitting [27], additionally it reduces the recombination rate of photogenerated $e^-$-$h^+$ pairs [28]. The characterization of the catalysts has been done by nitrogen adsorption, XRD, Raman and UV-Vis spectroscopies. The water splitting reaction has been carried out at room temperature using a water-ethanol solution irradiated with a high pressure of mercury lamp. Ethanol reacts with the photogenerated holes which is an irreversible reaction performed on the semiconductor surface and the photocatalytic activity toward reduction of water to produce hydrogen is improved [29].

## 2. Experimental

### 2.1 Catalyst preparation

The nanostructured $TiO_2$-CoO and $TiO_2$-$WO_3$ samples were prepared by the sol-gel method using titanium (IV) butoxide (Aldrich 97%), cobalt nitrate (Reasol 99%) and tungstic acid (Fluka 99%) as precursors: 44 mL of 1-butanol (Aldrich 99.4%) and 18 mL of distilled water containing the appropriated amount of $Co(NO_3).6H_2O$ to obtain solids with 1.0, 3.0, and 5.0 wt.%, were mixed and a few drops of $HNO_3$ were added in order to obtain pH=3 in the solution. After the solution was heated under reflux at 70°C and then 44 mL of titanium(IV) butoxide were added drop wise (water/alkoxide molar ratio 8) and maintaining during 4 h under magnetic stirring until the gel was formed. Afterwards, the gel was dried at 70°C during 24 h and the solid was ground to a fine powder in an agate mortar. The obtained xerogel was then annealed at 500°C during 5 h in static air atmosphere using a heating rate of 1°C/min; finally the product was ground again. As reference pure $TiO_2$ sample was prepared in the same way described above but with no adding the Co and W precursor.

### 2.2 Catalyst characterization

#### 2.2.1 Physisorption analysis

Nitrogen adsorption-desorption isotherms were obtained with an automatic Quantachrome Autosorb 3B instrument. Prior to the nitrogen adsorption, all the samples were outgassed overnight at 200° C. The specific surface areas of the samples were calculated from the nitrogen adsorption-desorption isotherms using the BET method, and the mean pore size diameter form the desorption isotherms using the BJH method.

#### 2.2.2 X-ray powder diffraction

The obtained powders $TiO_2$ and doped $TiO_2$-ZnO were analyzed by X-ray diffraction using a Bruker D-8 Advance apparatus. The diffraction intensity as a function of the diffraction angle ($2\theta$) was measured between 4 and 70°, using a step of 0.03° and a counting time of 0.3 s per step.

#### 2.2.3 Raman Spectroscpy

Los espectros Raman fueron obtenidos en un espectrómetro marca Renishaw, modelo MicroRaman Invia, utilizando un objetivo de 100X y como fuente de radiación monocromática un láser de Argón, con longitud de onda de emisión de 514.5 nm correspondiente a la luz verde, y una potencia de salida de 25 mW. En el equipo de análisis fueron colocados 10 mg de muestra en polvo de los sólidos. El intervalo de desplazamiento Raman para el análisis fue de 0 a 1200 $cm^{-1}$.

#### 2.2.4 Infrared FT-IR

The FT-IR studies were realized by IR-Shimadzu equipped with ATR, with a wavelength de 500 $cm^{-1}$ to 4000 $cm^{-1}$.

#### 2.2.5 UV-Vis diffuse reflectance spectroscopy

The UV–Vis absorption spectra were obtained with a Varian Cary 100 UV–Vis spectrophotometer coupled with an integration sphere for diffuse reflectance studies. A sample of MgO with a 100% reflectance was used as a reference. The diffuse reflectance spectrum was obtained and transformed to a magnitude proportional to the extinc-

tion coefficient (α) through the Kubelka-Munk function, Equation 1.

$$F(R) = \frac{(1-R)^2}{2R} \quad (1)$$

The Eg was then calculated from the plot of the modified Kubelka-Munk function F(R) vs wavelenght of the absorbed light.

### 2.2.6 Photocatalytic $H_2$ production

The photoactivity for the hydrogen generation was evaluated using a homemade Pyrex reactor of 200 mL containing an aqueous solution water-ethanol (1:1 molar ratio) and 0.1 g of catalysts. The photoirradiation was made using a high pressure Hg pen-lamp (with a radiation of 254 nm and intensity of 2.2 mW/cm$^2$) encapsulated in a quartz tube immersed in the water solution. The amount of hydrogen produced was followed by gas chromatography using a Varian CP-3800 gas chromatograph equipped with a thermal conductivity detector and with a molecular sieve 5A column (30m length, 0.35mm ID and 50 mm OD).

## 3. Results and discussion

### 3.1 Specific surface area

The specific surface areas of the samples annealed at 500° C are reported in Table 1. The results show that specific surface area by the BET method of the $TiO_2$-CoO and $TiO_2$-$WO_3$ semiconductors is higher than obtained with the bare $TiO_2$. As the amount of Co and W increases an increment in the specific surface area was observed. It increments from 90 to 95 m$^2$/g for the $TiO_2$-CoO and 48 to 91 m2/g for the $TiO_2$-WO3 solids respectively. This result suggest that the pores of $TiO_2$-CoO mixed oxide are cylinders perfect and present the same pore size, with $TiO_2$-$WO_3$ the result suggest that, it present an increase of width pore when the wt.% of W increase.

**Table 1**. Textural properties, band gap and $H_2$ production

| Catalysts (wt%) | Area m$^2$/g | Eg (eV) | $H_2$ Production (μmol/h) | Crystal Size D |
|---|---|---|---|---|
| Co 1.0 | 90 | 1.59 | 562 | 12 |
| Co 3.0 | 93 | 1.75 | 864 | 13 |
| Co 5.0 | 95 | 2.44 | 1008 | 14 |
| W 1.0 | 48 | 3.02 | 600 | 11 |
| W 3.0 | 53 | 3.12 | 884 | 12 |
| W 5.0 | 91 | 3.08 | 956 | 13 |
| $TiO_2$ | 64 | 3.2 | 190 | 7.2 |

### 3.2 X-ray diffraction

Figure 1 shows the X-ray diffraction patterns of the $TiO_2$ and 1.0, 3.0 and 5.0% cobalt oxide and tungsten oxide with $TiO_2$ samples. The nanocrystalline anatase structure was confirmed by (1 0 1), (0 0 4), (2 0 0), (1 0 5) and (2 1 1) diffraction peaks [30,33]. The XRD patterns of anatase have a main peak at 2θ = 25.2° corresponding to the 101 plane while the main peaks of rutile and brookite phases are at 2θ = 27.4° (110 plane) and 2θ = 30.8° (121 plane), respectively. Therefore, rutile and brookite phases have not been detected [31,32]. The XRD patterns didn't show any Co and W phase (even for 5% CoO-$TiO_2$ and $WO_3$-$TiO_2$ sample) indicating that Co and W ions are uniformly dispersed among the anatase crystallites [34,35]. In the region of 2θ = 10-80°, the shape of diffractive peaks of the crystal planes of pure $TiO_2$ (sample a) is quite similar to that of CoO-$TiO_2$ and $WO_3$-$TiO_2$ (samples b to g) with different concentrations of Co and W. The average particle size was estimated from the Scherrer equation on the anatase (2θ =25.2, 37.8, and 48.1°) diffraction peaks (the most intense peaks for each sample): $D = K\lambda / (\beta \cos \theta)$.

where D is the crystal size of the catalyst, λ the X-ray wavelength (1.54056 Å), β the full width at half

maximum of the diffraction peak (radian), Kα is a coefficient (0.89) and θ is the diffraction angle at the peak maximum. Average crystal sizes of $TiO_2$ and CoO-$TiO_2$ were calculated to be around 12-14 nm and 11-13 nm, respectively.

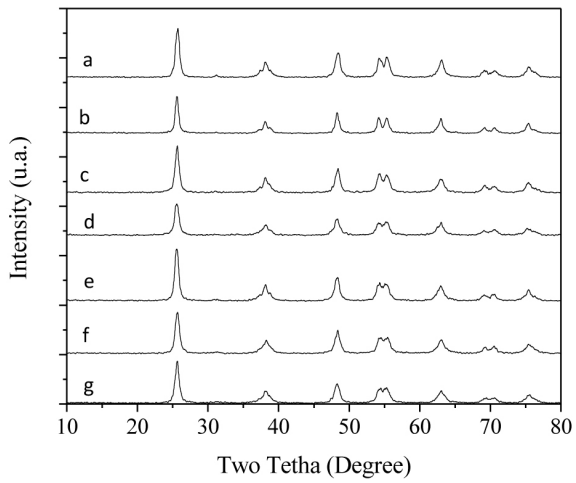


**Figure 1**. XRD of mixed oxide, $TiO_2$-CoO and $TiO_2$-$WO_3$. (a: $TiO_2$, b: CoO al 1.0 wt.%, c: CoO al 3.0 wt.%, d: CoO al 5.0 wt.% , e: $WO_3$ al 1.0 wt.%, f: $WO_3$ al 3.0 wt.%, g: $WO_3$ al 5.0 wt.%)

## 3.3 Raman spectroscopy

Raman spectra of all samples are represented in Figure 2 and were compared with those reported in the literatura [36,38]. You can appreciate four Raman peaks of anatase phase which are to 145.8 $cm^{-1}$, 397.9 $cm^{-1}$, 513 $cm^{-1}$ y 640.7 $cm^{-1}$; which are assigned to modes 2B1g and the mode 2Eg respectively. Also presented are confirmed in X-ray, as there is a decrease of the peaks increase as the content of CoO and $WO_3$.

## 3.3 FT-IR spectroscopy

FT-IR spectra of $TiO_2$ and 1.0, 3.0 and 5.0 wt.% Co and W samples (Figure 3) show peaks corresponding to stretching vibrations of the O-H and bending vibrations of the adsorbed water molecules. The intensity of these peaks in 3350-3450 cm-1 is lower because the annealing temperature which indicates the removal of a large portion of the adsorbed water from $TiO_2$ (not shown in the figure) [39]. The broad intense band below 1200 $cm^{-1}$ is due to Ti-O-Ti vibrations. The shift to the lower wavenumbers and sharpening of the Ti-O-Ti band from "b" to "g" in Figure 3 may be due to decrease in size of the catalyst nanoparticles with increasing Co and W in the formation of mixed oxide with the $TiO_2$ from 1% to 5.0%, respectively. In addition, the surface hydroxyl groups in $TiO_2$ increase with the increase of Co and W wt.%, which is confirmed by increase in intensity of the corresponding peaks. There is no band centered at 1389 $cm^{-1}$ due to the bending vibrations of the C-H bond in the catalysts of the mixed oxide [39]. Also, there are no excess bands assigned for the alkoxy groups.

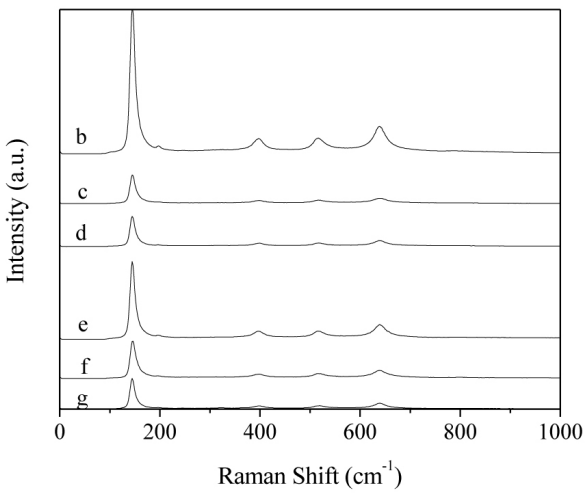


**Figure 2.** Spectrum Raman of mixed oxide, $TiO_2$-CoO and $TiO_2$-$WO_3$. (b: CoO al 1.0 wt.%, c: CoO al 3.0 wt.%, d: CoO al 5.0 wt.% , e: $WO_3$ al 1.0 wt.%, f: $WO_3$ al 3.0 wt.%, g: $WO_3$ al 5.0 wt.%)

## 3.4 UV-Vis Diffuse reflectance spectroscopy (DRS)

The electronic bands of the different titania samples were studied whose corresponding spectra are provided in Figure 3. The absorption spectrum of $TiO_2$ consists of a single broad intense absorption around 400 nm due to the charge-transfer from the valence band (mainly formed by 2p orbitals of the oxide anions) to the conduction band (mainly formed by 3d t2g orbitals of the $Ti^{4+}$ cations) [40]. This absorption is similar to $TiO_2$-$WO_3$ mixed oxide be-

cause present a spectrum to 400 nm. The $TiO_2$ and $WO_3$-$TiO_2$ mixed oxide showed absorbance in the shorter wavelength region while CoO-$TiO_2$ and the DRS results showed a red shift in the absorption onset value in the case of CoO added titania. The mixed oxide of various transitional metal ions into $TiO_2$ could shift its optical absorption edge from UV into visible light range, but no prominent change in $TiO_2$ band gap was observed [34].

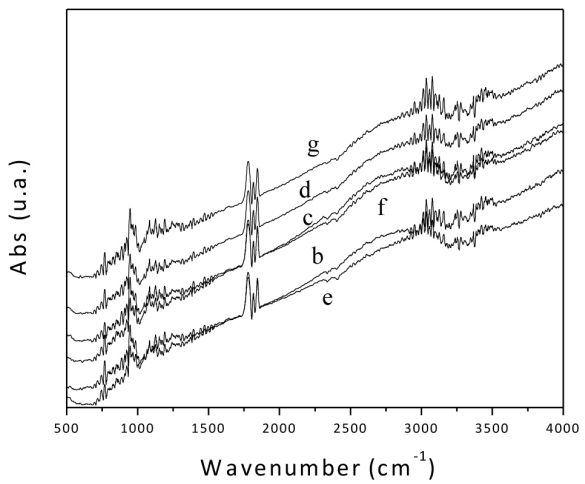


**Figure 3**. FT-IR spectrum of $TiO_2$, $TiO_2$-CoO and $TiO_2$-$WO_3$. (b: CoO al 1.0 wt.%, c: CoO al 3.0 wt.%, d: CoO al 5.0 wt.%, e: WO3 al 1.0 wt.%, f: $WO_3$ al 3.0 wt.%, g: $WO_3$ al 5.0 wt.%)

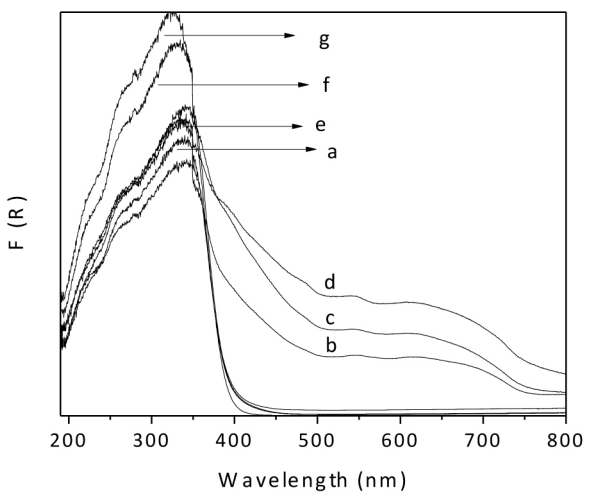


**Figure 4.** DRS spectrum of $TiO_2$, $TiO_2$-CoO and $TiO_2$-$WO_3$. (a: $TiO_2$, b: CoO al 1.0 wt.%, c: CoO al 3.0 wt.%, d: CoO al 5.0 wt.% , e: $WO_3$ al 1.0 wt.%, f: $WO_3$ al 3.0 wt.%, g: $WO_3$ al 5.0 wt.%)

Figure 5 shows the spectroscopy of $TiO_2$-CoO samples before of reaction, where the base line was realized with $TiO_2$ and it indicates that its absorbance is 750 nm with the $TiO_2$-CoO all the samples, when increases CoO content there is a displacement to 372 nm for the $TiO_2$-CoO with 3.0 and 5.0 wt% and this form we verified that CoO is disperse in the titania lattice. The same procedure for the $WO_3$ was realized, see Figure 5**,** where it show two peaks in 362 nm with 1.0 wt%, when increase $WO_3$ content there is a displacement to 369 nm and 375 nm for the samples with content 3.0 and 5.0 wt% respectively. The second peaks are in the region of 400 nm to 450 nm that suggest a formation of Plasmon.

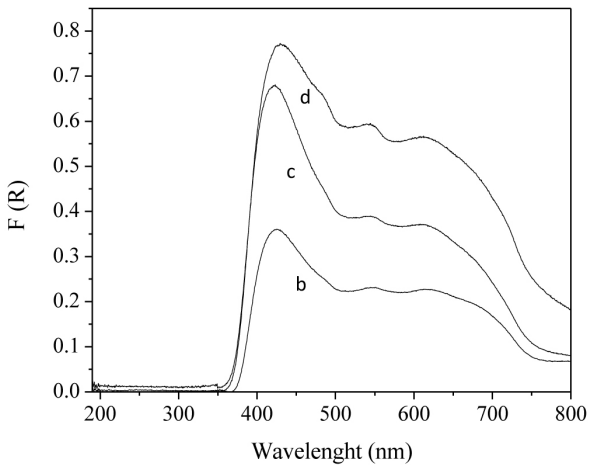


**Figure 5**. DRS image of $TiO_2$-CoO. ( b: CoO al 1.0 wt.%, c: CoO al 3.0 wt.%, d: CoO al 5.0 wt.%)

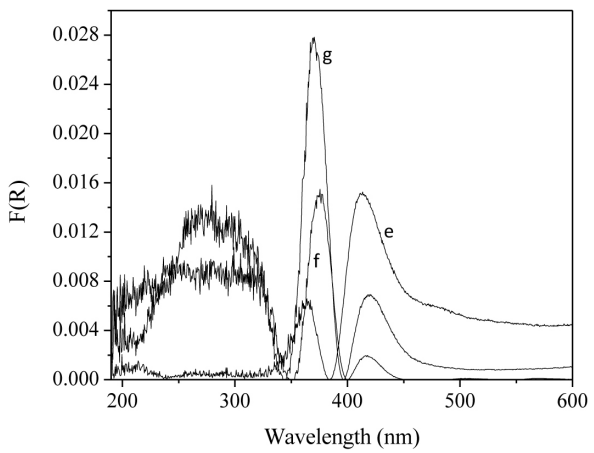


**Figure 6**. DRS image of $TiO_2$-$WO_3$. (e: $WO_3$ al 1.0 wt.%, f: $WO_3$ al 3.0 wt.%, g: $WO_3$ al 5.0 wt.%)

The Figure 7 spectra, was obtained on powders after reaction. The analysis shows that at 225 nm probably exist a transition of the catalyst of $Ti^{4+}$ to $Ti^{3+}$, but in the region of 362 to 375 nm where $WO_3$ is present, only Co with 1.0 wt% present a little change (sample e), the peaks after of reaction diminished that confirm change in the material of $TiO_2$-$WO_3$ samples. With respect to $TiO_2$-CoO samples this present a little change in the region of 544 nm, which suggest that there are a change $Co^{2+}$ to $Co^{3+}$. In the region of 400 to 500 nm present change significatives that suggest the $TiO_2$-CoO samples aren´t changes.

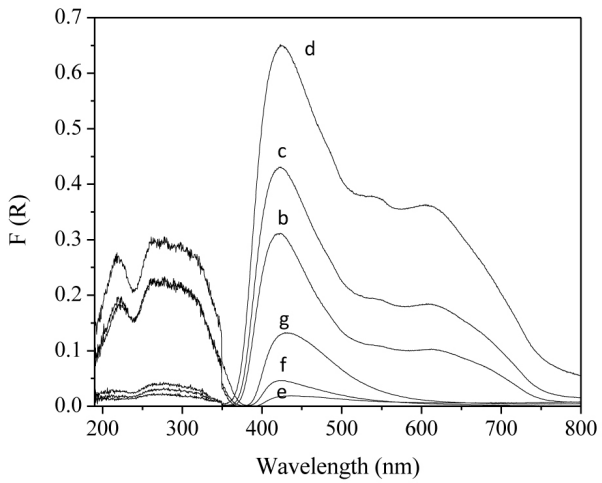


**Figure 7.** DRS spectrum, after of reaction CoO and $WO_3$. ( b: CoO 1.0 wt.%, c: CoO 3.0 wt.%, d: CoO 5.0 wt.% , e: $WO_3$ 1.0 wt.%, f: $WO_3$ 3.0 wt.%, g: $WO_3$ 5.0 wt.%)

Figure 8 shows the hydrogen production as a function of the irradiation time for bare $TiO_2$, $TiO_2$-CoO and $TiO_2$-$WO_3$. It can be seen that the hydrogen formation increases with the Co and W wt. %. The hydrogen production from bare TiO2 was 190 μmol/h. An important effect of cobalt oxide is observed, the $H_2$ formation for $TiO_2$-CoO and $TiO_2$-$WO_3$ with 5 wt% was 900 and 1000 μmol/h, respectively, an increase of 500 percent approximately. In this case of the above 5 wt. % CoO and $WO_3$ is the key to improved hydrogen photocatalytic production. This results are very interesting compared when is used titania nanotubes with Ir and Co [41] nanocomposites of CoO [42], Pt loaded $TiO_2$ [43] $WO_3$-$TiO_2$ [44].

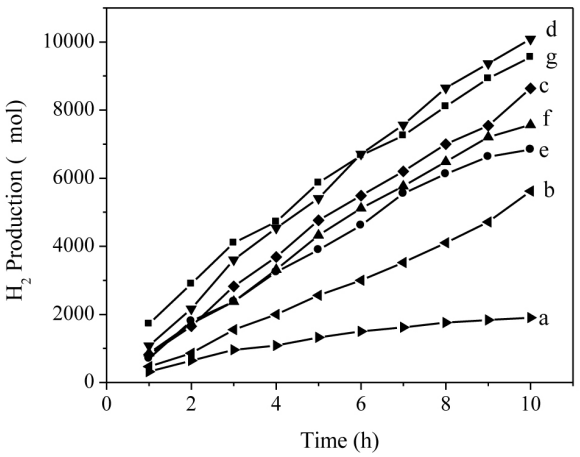


**Figure 8**. Profile of $H_2$ production with $TiO_2$, $TiO_2$-CoO and $TiO_2$-$WO_3$. (a: $TiO_2$, b: CoO 1.0 wt.%, c: CoO 3.0 wt.%, d: CoO 5.0 wt.% , e: $WO_3$ 1.0 wt.%, f: $WO_3$ 3.0 wt.%, g: $WO_3$ 5.0 wt.%)

## 4. Conclusions

$TiO_2$, $TiO_2$-CoO and $TiO_2$-$WO_3$ nanoparticles were prepared by the sol-gel method. From among all of the samples only anatase phase was confirmed from the XRD results. From the XRD, UV-Vis and FT-IR results, it was confirmed that the incorporation of Co and W in $TiO_2$ decreases the grain size, shifts the absorption to higher wavelenghts (red shift) and lowers the surface area due to agglomeration of the particles. The photocatalytic activity of hydrogen production under UV irradiation revealed higher activity in the presence of the mixed oxide. Among the Co and W samples, the catalyst exhibited the highest photocatalytic activity, while under visible irradiation, the best catalyst was the 5.0% $TiO_2$-CoO.

## References


1. N. Arai, N. Saito, H. Nishiyama, K. Domen, H. Kobayashi, K. Sato, Y. Inoue. Catal.Today., 129, 407, (2007).
2. S. Shen, L. Zhao, L. Guo. Int. J. Hydrogen Energy 35, 10148, (2010).
3. X. Zhang, D. Jing, L. Guo. Int. J. Hydrogen

Energy 35, 7051 (2010).
4. Jiři Zitaa, Josef Krýsa, Urh Cěrnigoj, Urška Lavrenčič-Štangar, Jaromir Jirkovsky´c, Jiři Rathouský. Catalysis Today 161, 29-34 (2011).
5. María L. Satuf, María J. Pierrestegui, Lorena Rossini, Rodolfo J. Brandi, Orlando M. Alfano. Catalysis Today 161, 121-126 (2011).
6. Yao-Hsuan Tseng, Chien-HungKuo. Catal. Today (2011), doi:10.1016/ j.cattod.2011.02.011.
7. M. Uzunova-Bujnova, R. Kralchevska, M. Milanova, R. Todorovska, D. Hristova, D. Todorovsky. Catalysis Today 151, 14-20 (2010).
8. Sylwia Mozia. Catalysis Today 156, 198-207 (2010).
9. C.A. Castro-López, A. Centeno, S.A. Giraldo. Catalysis Today 157, 119-124 (2010).
10. V. Rodríguez-González, M.A. Ruiz-Gómez, L.M. Torres-Martínez, R. Zanella, R. Gómez. Catalysis Today 148, 109-114 (2009).
11. Adrián M.T. Silva, Cláudia G. Silva, Goran Drazic, Joaquim L. Faria. Catalysis Today 144, 13-18 (2009).
12. A. Kubacka, G. Colón, M. Fernández-García. Catalysis Today 143, 286-292 (2009).
13. C. Guzmán, G. del Ángel, R. Gómez, F. Galindo-Hernández, C. Ángeles-Chavez.
14. Rosendo López, Ricardo Gómez, María Elena Llanos. Catalysis Today 148, 103-108 (2009).
15. Claudia L. Bianchi, Giuseppe Cappelletti, Silvia Ardizzone, Stefano Gialanella, Alberto Naldoni, Cesare Oliva, Carlo Pirola. Catalysis Today 144, 31-36 (2009).
16. A. Bernabeu, R.F. Vercher, L. Santos-Juanes, P.J. Simón, C. Lardín, M.A. Martínez, J.A. Vicente, R. González, C. Llosá, A. Arques, A.M. Amat. Solar photocatalysis as a tertiary treatment to remove emerging pollutants from wastewater treatment plant effluents. Catalysis Today 161 (2011) 235–240.
17. Pow-Seng Yapa, Teik-Thye Lima, Madhavi Srinivasan. Nitrogen-doped $TiO_2$/AC bifunctional composite prepared by two-stage calcination for enhanced synergistic removal of hydrophobic pollutant using solar irradiation. Catalysis Today 161 (2011) 46–52.
18. Tseng IH, Jeffrey CSW. Chemical states of metal-loaded titania in the photoreduction of $CO_2$. Catal. Today, 97 (2004) 113–9.
19. Sreethawong S, Suzuki Y, Yoshikawa S. Photocatalytic evolution of hydrogen over mesoporous $TiO_2$ supported NiO photocatalyst prepared by single step sol–gel process with surfactant template. Int J Hydrogen Energy 30 (2005) 1053–62.
20. András Erdóelyi, János Raskó, Tamara Kecskés, Mariann Tóth, Márta Dömök, Kornélia Baán. Hydrogen formation in ethanol reforming on supported noble metal catalysts. Catalysis Today 116 (2006) 367–376.
21. L.S. Yoong a, F.K. Chong a, Binay K. Dutta. Development of copper-doped $TiO_2$ photocatalyst for hydrogen production under visible light. Energy 34 (2009) 1652–1661.
22. Deborah V. César, Rachel F. Robertson, Neuman S. Resende. Characterization of ZnO and $TiO_2$ catalysts to hydrogen production using thermoprogrammed desorption of methanol. Catalysis Today 133–135 (2008) 136–141.
23. Thammanoon Sreethawong, Yoshikazu Suzuki, Susumu Yoshikawa, Photocatalytic evolution of hydrogen over mesoporous $TiO_2$ supported NiO photocatalyst prepared by single-step sol–gel process with surfactant template. International Journal of Hydrogen Energy 30 (2005) 1053 – 1062.
24. Félix Galindo-Hernández, Ricardo Gómez. Degradation of the herbicide 2,4-dichlorophenoxyacetic acid over $TiO_2$–$CeO_2$ sol–gel photocatalysts: Effect of the annealing temperature on the photoactivity. Journal of Photochemistry and Photobiology A: Chemistry 217 (2011) 383–388.
25. I. Nakamura, N. Negishi, S. Kutsuna, T. Ihara, S. Sugihara, K. Takeuch, Role of oxygen vacancy in the plasma-treated $TiO_2$ photocatalyst with visible light activity for NO removal, J. Mol. Catal. A: Chem. 161 (2000) 205–212.
26. T. Ihara, M. Miyoshi, Y. Iriyama, O. Matsumoto, S. Sugihara, Visible-light-active titanium oxide photocatalyst realized by an oxygen-deficient structure and by nitrogen doping, Appl. Catal. B: Environ. 42 (2003) 403–409.

27. Shama Rehman, Ruh Ullah, A.M. Butt, N.D. Gohar. Strategies of making $TiO_2$ and ZnO visible light active. Journal of Hazardous Materials, 170 (2009) 560–569.
28. R.M. Navarro, F. del Valle, J.A. Villoria de la Mano, M.C. Álvarez-Galván, J.L.G. Fierro. Photocatalytic wáter splitting under visible light: Concept and catalysts development. Advances in Chemical Engineering, 36 (2009) 111-141.
29. Bandara J, Udawatta CPK, Rajapakse CSK. Highly stable CuO incorporated $TiO_2$ catalyst for photocatalytic hydrogen production from $H_2O$. Photochem Photobiol Sci, 4 (2005) 857–61.
30. H. Ogawa, A. Abe, J. Electrochem. Soc. 128 (1981) 685.
31. K.V. Baiju, P. Shajesh, W. Wunderlich, P. Mukundan, S.R. Kumar, K.G.K. Warrier, J. Mol. Catal. A 276 (2007) 41.
32. K.M.K. Srivatsa, M. Bera, A. Basu, Thin Solid Films 516 (2008) 7443.
33. V. Chakrapani, J. Thangala, M. Sunkara. $WO_3$ and W2N nanowire arrays for photoelectrochemical hydrogen production. Int. J. of Hydrogen Energy 34 (2009) 9050-9059.
34. J.C.S. Wu, C.H. Chen, J. Photochem. Photobiol. A 163 (2004) 509.
35. L. Chen, J. Li, M. Ge, R.Zhu. Catalytis today 153 (2010)
36. W. F. Zhang, Y. L. He, M. S. Zhang, Z. Yin, Q. Chen, J. Phys. D: Appl. Phys. 33 (2000) 912.
37. K. Ishikawa, K. Yoshikawa, N. Okada, Phys. Rev. B, 37 (1988) 5852.
38. T. Ohsaka, F. Izumi, Y. Fujiki, J. Raman Spectroscopy, 7 (1978) 321
39. W. Hung, S. Fu, J. Tseng, H. Chu, T. Ko, Chemosphere 66 (2007) 2142
40. N. Venkatachalam, M. Palanichamy, V. Murugesan, J. Mol. Catal. A 273 (2007) 177.
41. M. A. Khan, O.B. Yang. Photocatalytic water splitting fro hydrogen production under visible light on Ir and Co ionized titania nanotube. Catalysis Today 146 (2009) 177-182.
42. J. Yan, H. Yang, Y. Tang, Z. Lu, S. Zheng, M. Yao, Y. Han. Synthesis and photocatalytic activity of $CoYyFe_{2-y}O_4$-$CuCO_2O_4$ nanocomposites for $H_2$ production under visible light irradiation. Renewable Energy 34 (2009) 2399-2403.
43. Tao Chen, Zhaochi Feng, Guopeng Wu, Jianying Shi, Guijun Ma, Pinliang Ying, and Can Li. J. Phys. Chem. C, 2007, 111, 8005-8014.